

Cross-plane thermal conductivity of GaN/AlN superlattices

Anna Spindlberger,^{a)} Dmytro Kyslychyn, Lukas Thumfart, Rajdeep Adhikari, Armando Rastelli, and Alberta Bonanni^{a)}

Institute of Semiconductor and Solid-State Physics, Johannes Kepler University Linz, Altenbergerstr. 69, 4040 Linz, Austria

(Dated: 14 October 2021)

Heterostructures consisting of alternating GaN/AlN epitaxial layers represent the building-blocks of state-of-the-art devices employed for active cooling and energy-saving lightning. Insights into the heat conduction of these structures are essential in the perspective of improving the heat management for prospective applications. Here, the cross-plane (perpendicular to the sample's surface) thermal conductivity of GaN/AlN superlattices as a function of the layers' thickness is established by employing the 3ω -method. Moreover, the role of interdiffusion at the interfaces on the phonon scattering is taken into account in the modelling and data treatment. It is found, that the cross-plane thermal conductivity of the epitaxial heterostructures can be driven to values as low as $5.9 \text{ W}/(\text{m} \cdot \text{K})$ comparable with those reported for amorphous films, thus opening wide perspectives for optimized heat management in III-nitride-based epitaxial multilayers.

The tuneable bandgap, high thermal stability, high electric field strength, high electron mobility, and the presence of a spontaneous and piezoelectric polarization in wurtzite III-nitrides led to the integration of GaN and its alloys in state-of-the-art electronics technology¹. Current III-nitride based devices range from light emitting diodes in the ultraviolet^{2,3} and visible range^{4,5} to high-electron mobility transistors⁶⁻⁸ and biosensors⁹. Another research field involving III-nitrides is opened up by doping them with transition metals and by studying the emergent spin related phenomena¹⁰⁻¹³. Generally, devices experience efficiency losses due to internal heating^{14,15} and low thermal conductivity materials are needed as the basis for thermoelectric devices^{16,17} or for on-device cooling¹⁸. Thus, a detailed understanding of the thermal properties of thin films and nitride based heterostructures is mandatory in the perspective of efficient thermal management.

Previous works have investigated the thermal conductivity of III-nitrides in bulk¹⁹ and in thin films²⁰ in detail. Furthermore, several groups studied the decrease of thermal conductivity with increasing Al concentration in $\text{Al}_x\text{Ga}_{1-x}\text{N}$ bulk²¹ and thin films^{20,22-25}. A decrease of the bulk thermal conductivity of III-nitrides due to impurity doping²⁶⁻²⁹ was also found, while an enhanced conductivity is reported for isotopically enriched GaN³⁰. For AlN/GaN stacks, significant changes in the phonon properties due to interface effects³¹⁻³⁴ and strain³⁵ were reported, while for compositionally graded interfaces it was found that alloy scattering is dominant over mismatch scattering³⁶ of phonons.

In order to minimize the thermal conductivity of a heterostructure, either the thickness of the single layers must be reduced or scattering centers are introduced by interdiffusion. For instance, in the case of $\text{Al}_{0.4}\text{Ga}_{0.6}\text{N}$, the cross-plane (perpendicular to the sample's surface) thermal conductivity κ_{\perp} is theoretically predicted to decrease to $1 \text{ W}/(\text{m} \cdot \text{K})$ ²² when reducing the layer thickness down to 2 nm. Due to

the anisotropy of the thermal conductivity tensor, the in-plane component κ_{\parallel} of the thermal conductivity is expected to exhibit a different heat conduction than the cross-plane one³⁷. The interface resistance affects the interface crossing of phonons and leads to a quenching of the thermal conductivity, as reported for Ge/Si superlattices³⁸⁻⁴⁰ and for up to eight pairs of AlN/GaN multilayers⁴¹.

In this work, the thermal conductivity of heterostructures consisting of up to 50 GaN/AlN pairs with different layer

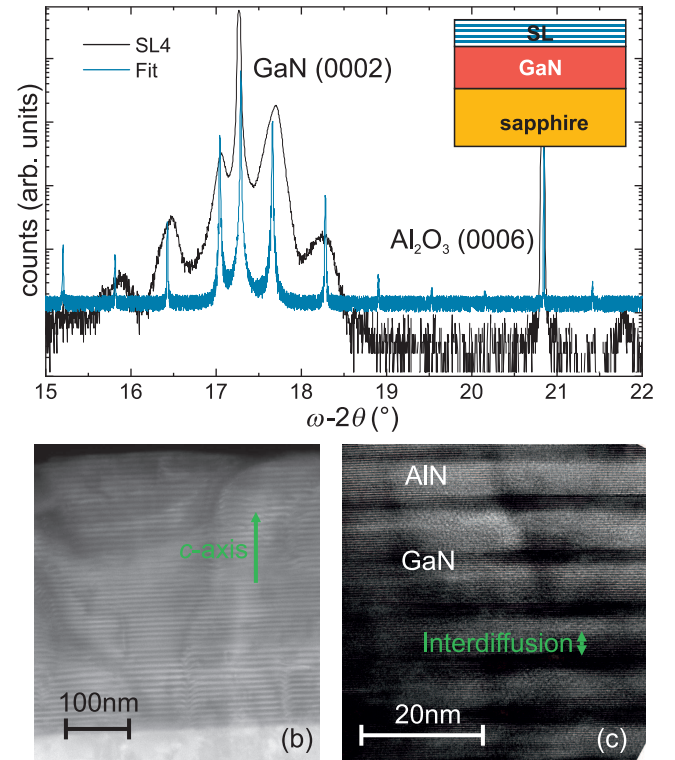


FIG. 1. (a) XRD scan around the GaN (0002) for SL4 and the fitted signal. Inset: schematic sample structure. HAADF image of the SL4: (b) the whole structure and (c) a magnified image of the interdiffusion region between GaN and AlN.

^{a)} Authors to whom correspondence should be addressed: anna.spindlberger@jku.at and alberta.bonanni@jku.at

thickness is measured by the differential 3ω -method^{42,43} and simulated with *ab-initio* calculations.

The investigated samples are grown by metal organic vapor phase epitaxy (MOVPE) according to the procedure detailed in the supplementary material. In particular, all samples are grown on a *c*-sapphire substrate, upon deposition of a low temperature nucleation layer followed by a 1.5 μm thick GaN buffer layer and a GaN/AlN superlattice (SL). The considered samples, together with their relevant parameters are listed in Table I. The SL heterostructures consist of 50 GaN/AlN pairs. The thicknesses of each GaN and AlN layer is varied between 4 nm and 16 nm over the sample series, covering typical thicknesses for GaN/AlN quantum wells⁴⁴ and the number of layers needed for high-reflectivity bands of distributed Bragg mirrors^{45,46}. A sketch of the SL structure is given in the inset to FIG. 1 (a) and in the following the SLs are indicated by SL4, SL8, SL12, SL16, where the numbers refer to the thickness of the single layers in nm. Additionally, two reference samples, namely a clean sapphire substrate and a GaN buffer, are also included in the study.

The crystallographic properties are analysed by high-resolution x-ray diffraction (XRD) and transmission electron microscopy (TEM). In FIG. 1 (a), the $\omega - 2\theta$ scan of the SL4 around the GaN (0002) reflection is plotted and the signal simulated with the AMASS software from PANalytical is given. The satellite peaks of the main GaN reflection arise due to the interference in the diffraction of the different layers of the multi-layer structure. The individual layers of the SL are evidenced in the high-angle annular dark-field image (HAADF), given for sample SL4 in FIG. 1 (b). The upward arrow indicates the growth direction. Due to interdiffusion, the interfaces between the GaN and the AlN layers are smeared out in an $\text{Al}_x\text{Ga}_{1-x}\text{N}$ layer⁴⁷, as evidenced by the EDX measurements shown in FIGs. S3 (a) and (b) of the supplementary material and marked by the arrow in FIG. 1 (c). The interdiffusion at the interface can suppress the coherent nature of phonons, favours diffusive scattering and influences the cross-plane heat conduction^{37,41,48,49}. The detailed analysis of the layers' thickness with TEM and XRD can be found in the supplementary material, where the TEM images in FIG. S2 (a)-(d) display V-shaped defects also reported in previous works⁵⁰.

For the thermal conductivity measurements, a 60 nm thin insulating AlO_x layer is deposited onto the specimens, followed by a metal structure consisting of a 120 nm-thick and 10 μm wide Au layer, which is used for heating the underlying material and for determining the corresponding temperature rise. The fabrication steps and geometry of the contacts are given in the section II.C of the supplementary material.

Measurements of the cross-plane thermal conductivity κ_\perp are performed with the differential 3ω -method⁴² in the temperature range between 160 K and 455 K. First the thermal conductivity κ_\perp of the sapphire substrate and of the GaN buffer layer are measured. The obtained values serve as references for the thermal conductivity for the SLs, as their influence on the measurement have to be deducted. The data evaluation is carried out by solving the heat diffusion equation in a matrix formalism and by fitting the measured temperature os-

TABLE I. Samples' details including layer thickness, effective thermal conductivity $\kappa_{3\omega}$ and simulated thermal conductivity κ_{sim} at 300 K.

sample	layer thickness (nm)	$\kappa_{3\omega}$ (W/(m · K))	κ_{sim} (W/(m · K))
sapphire	330000	38.0	34.6
GaN	1500	213.4	120.1
SL4	4/4	5.9 ^a	5.6 ^b
SL8	8/8	6.4 ^a	6.1 ^b
SL12	12/12	8.2 ^a	6.7 ^b
SL16	16/16	10.1 ^a	7.1 ^b

^a SL with 50 GaN/AlN pairs

^b simulated SL with five GaN/AlN pairs

cillations as a function of the heater frequency⁵¹. The whole SL is treated as a single layer.

The measured cross-plane thermal conductivity of the clean substrate and of the buffer deposited onto the substrate as a function of temperature T in the interval (160–455) K are plotted as symbols in FIG. 2 (a) and the values for room temperature are included in Table I. The simulated conductivity *versus* temperature of the reference samples is also given in FIG. 2 (a). The theoretical calculations for the sapphire substrate are performed following the procedure by Burghartz *et al.*⁵² with a sapphire thickness of 330 μm and a temperature dependent specific heat capacity taken from Ref. [53]. The values of the measured sapphire substrate follow the trend

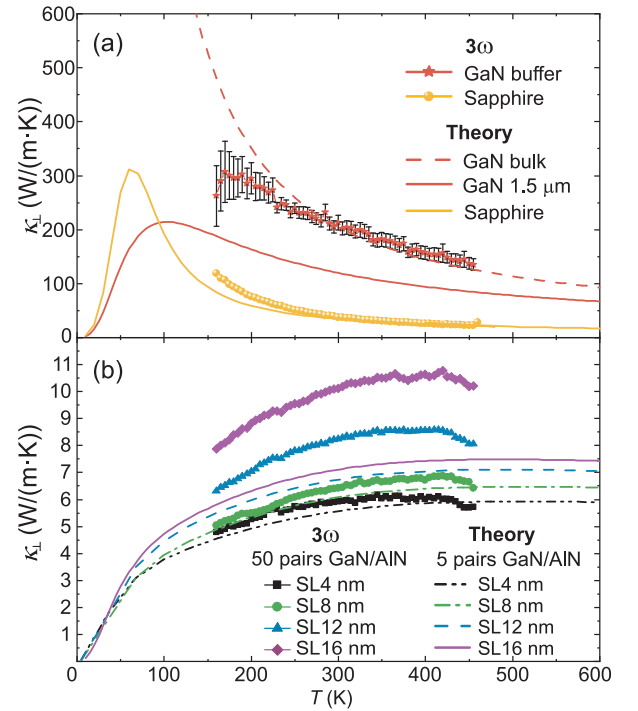


FIG. 2. (a) Cross-plane thermal conductivity κ_\perp of the reference samples, sapphire substrate and substrate + GaN buffer, and (b) of the 4 SLs as measured with the differential 3ω -method (symbols) and simulated (line).

of the simulated conductivity up to 200 K. The measured GaN film thermal conductivity slightly increases for decreasing temperatures and does not feature the steep slope below 200 K, that would be expected for bulk GaN.

The measured cross-plane thermal conductivity as a function of T of the four considered samples containing SLs is reported in FIG. 2 (b) and the obtained values at room temperature are collected in Table I. For the SL4 with the thinnest individual layers also the lowest thermal conductivity of $5.9 \text{ W}/(\text{m} \cdot \text{K})$ at 300 K is measured, while for the SL16 the thermal conductivity reaches $10.1 \text{ W}/(\text{m} \cdot \text{K})$ at the same temperature. The measured signal is mainly influenced by the SL and by the substrate, while the contribution of the buffer layer is negligible for the investigated samples, leading to an error on the measurements lower than 1.5 % over the whole temperature range. A decrease in thermal conductivity with decreasing temperature is found. In addition to the experiments, theoretical simulation accounting for phonon scattering mechanisms are performed and included as lines in FIG. 2 (b).

The calculations of the bulk GaN and GaN/AlN SL thermal conductivity are performed with the *almaBTE* software package⁵⁴ in the relaxation time approximation (RTA) and with an uniform wavevector grid of 24^3 . Further details about the program can be found in section III of the supplementary material. First, the temperature dependent thermal conductivity parallel to the c -axis of GaN is analysed. The simulated results are plotted in FIG. 3, where the topmost curve is the calculated conductivity for bulk GaN. The same simulation results are included for comparison in FIG. 2 (a) (solid line). The simulations are repeated for several layer thicknesses ranging from $0.01 \mu\text{m}$ to $100 \mu\text{m}$. The thickness of the MOVPE grown GaN buffer is $1.5 \mu\text{m}$, therefore a simulation of a GaN layer with the same thickness is included as line combined with reverse triangles in FIG. 3 and as dashed line in FIG. 2 (a). The κ_{\perp} conductivity of GaN reaches a maximum at 100 K for a film thickness of $1.5 \mu\text{m}$, and for thicker layers this maximum is shifted to lower temperatures, namely around 15 K for bulk GaN. Inyushkin *et al.*¹⁹ reported a maximum of $3770 \text{ W}/(\text{m} \cdot \text{K})$ around 28 K. No sharp maximum is reached for films with thicknesses of $1 \mu\text{m}$ and lower, for which, instead, the conductivity saturates at temperatures above 100 K. The highest reached thermal conductivity decreases with decreasing layer thickness, due to the significant effect of interface- and boundary-scattering of phonons.

Two limit regimes of heat conduction are relevant for crystalline films. In particular, in films with thicknesses much lower than the cross-plane mean free path λ_{dom} ²² of phonons, which depends on the cross-plane bulk thermal conductivity and on the mean free path of the cross-plane projection, κ_{\perp} is predominantly ballistic. In contrast, for films with film thickness much larger than λ_{dom} , the heat conduction is quasi-diffusive and therefore no distinct dependence on the film thickness is found. The film thicknesses considered in this work are smaller than the characteristic lengths²² for the transition to the ballistic regime, thus a distinct change of κ_{\perp} with different individual layer thicknesses is expected.

In order to gain further insights into the effect of alloy scattering, first a heterostructure is simulated, which assumes a

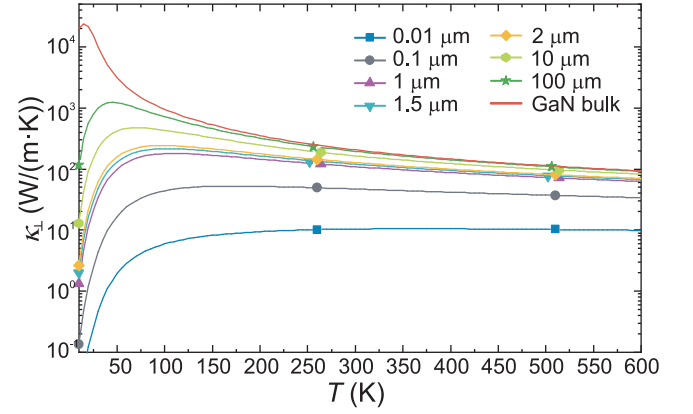


FIG. 3. Simulated bulk and thin film cross-plane thermal conductivity of GaN as a function of temperature T .

well defined stoichiometry of the GaN/AlN layers without intermixing and without a substrate. This ideal structure has a concentration x of Al of either 0 or 1. The SL crystal structure is built with the superlattice package of the *almaBTE* software, following the procedure reported in Ref. [38]. In FIG. 4 (a), the computed temperature dependent cross-plane thermal conductivity of the SL4 for one to 15 pairs of GaN/AlN is given. The thermal conductivity increases over the whole temperature range with increasing number of SL pairs. For completeness, also an inverse structure AlN/GaN (not shown), is calculated for five pairs, and the same thermal conductivity as in

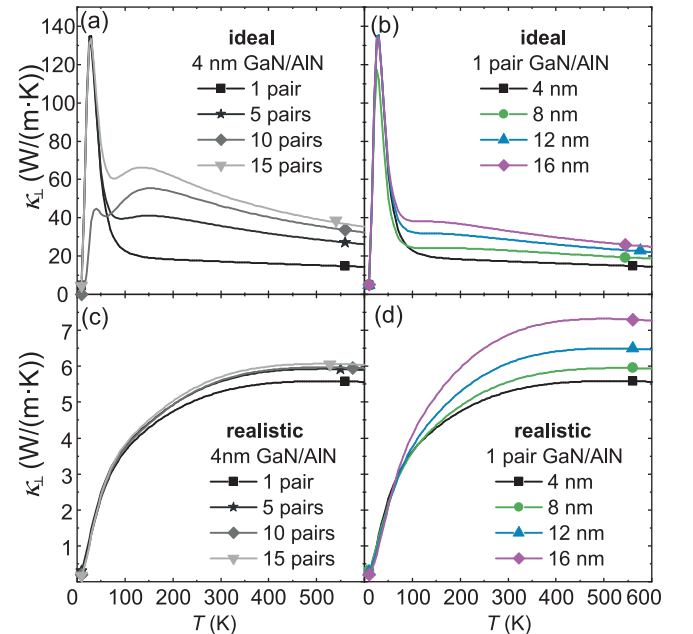


FIG. 4. Simulated temperature dependent thermal conductivity of an ideal GaN/AlN superlattice for (a) different number of pairs with 4 nm and (b) several layer thicknesses with one pair. Temperature dependent simulation of realistic SLs (c) with individual layer thickness of 4 nm with different number of pairs over the series and (d) one single pair with different thicknesses over the samples' series.

the case of the GaN/AlN sequence is found. In FIG. 4 (b), the simulated κ_{\perp} of one SL pair for all four thicknesses of the individual layer, *i.e.* 4 nm, 8 nm, 12 nm and 16 nm, are reported over temperature. The effect of scattering of phonons at interfaces is less pronounced with increasing layer thickness, leading to an increase in thermal conductivity^{55,56}, as evidenced in FIG. 4 (b).

In order to account for interdiffusion at the interfaces, a concentration-graded layer of $\text{Al}_x\text{Ga}_{1-x}\text{N}$ between the two ideal AlN and GaN layers is introduced in the calculations (realistic structures), while the total thickness of the structure is kept constant. In FIG. 4 (c), κ_{\perp} over the temperature is given for SL4 with different number of pairs over the samples' series. When comparing the simulated ideal structures with those including $\text{Al}_x\text{Ga}_{1-x}\text{N}$ regions, a significant decrease in thermal conductivity is found. In the realistic structures, additionally to the phonon interface scattering, alloy scattering is observed. As reported by Vermeersch *et al.*²² the change of Al concentration from GaN towards AlN leads to a decrease in the thermal conductivity of up to one order of magnitude in bulk materials. The increase in the number of layers slightly increases the thermal conductivity of the whole structure, in accord to Ref. [57]. In FIG. 4 (d) the conductivity of one GaN/AlN pair with intermixing for the four thicknesses is plotted over temperature. As found in the case of ideal SLs, the increase of an individual layer thickness induces an increment of the thermal conductivity. The thermal conductivity of the realistic SLs is less influenced by a change in layer numbers than by an increase of individual layer thickness. The simulations of five realistic GaN/AlN pairs qualitatively reproduce the shape of the measured κ_{\perp} given in FIG. 2 (b). As discussed, a slight increase in the maximum value of the thermal conductivity is expected when increasing the number of pairs from five to 50. Additional changes in the thermal conductivity can arise by a variance in the Al concentration and increases when going towards an ideal SL. The simulations do not consider any kind of defects, though the V-shaped ones, present in the MOVPE grown samples, are expected to reduce the thermal conductivity. Additionally, the simulations do not contain a substrate, which is expected to influence the phonon transport at the substrate and SL boundary. Furthermore, the influence of strain, predicted to increase the thermal conductivity³², in the layers is not treated in the simulations.

In semiconductors, thermal energy is mainly transported by phonons and the phonon frequency spectra can be used to identify the main scattering mechanism. In FIG. 5, the fraction of the normalized cumulative thermal conductivity, obtained by dividing the cumulative thermal conductivity by the bulk thermal conductivity transferred by phonons as a function of the frequency is given at 300 K. The simulated phonon contribution for a bulk GaN is plotted as a solid line. Moreover, the four lines with symbols represent the simulations for one pair of GaN/AlN with ideal and realistic composition and five pairs of GaN/AlN with ideal and realistic composition, respectively. For realistic SLs, a major contribution to the heat conductivity originates from phonons with frequency between 0 THz and 6 THz, while phonons between 12 THz and 16 THz contribute minimally, leading to a first plateau marked by the

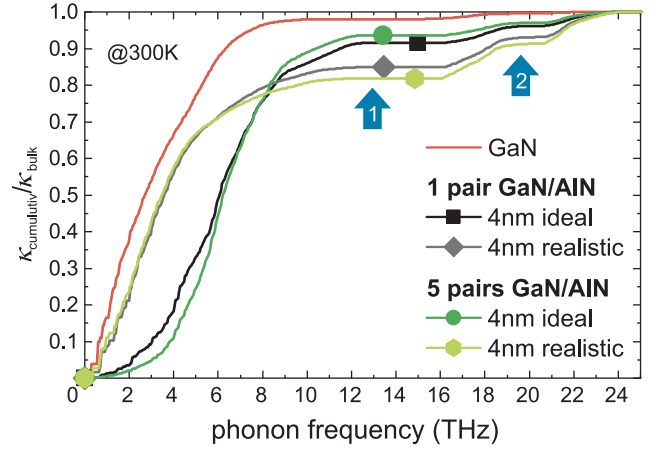


FIG. 5. Normalized cumulative thermal conductivity over the contributing phonon frequencies for realistic and ideal SLs.

upward arrow labeled with 1 in FIG. 5. A second plateau occurs above 19 THz, indicated by the upward arrow two, and phonons with frequencies higher than 22 THz do not contribute significantly to the thermal conductivity. The splitting in two plateaus is due to the alloy scattering of high-frequency phonons³⁸. Due to an enhancement of low-frequency phonon scattering at the abrupt interfaces³⁸, the conductivity of the ideal SLs is less significantly affected by phonons in the frequency range (0–4) THz. Only one prominent plateau above 8 THz is visible, due to the missing effect of alloy scattering. For completeness, the simulated cumulative thermal conductivity normalized to the bulk is provided as a function of the mean free path (MFP) of the phonons for bulk AlN, bulk GaN, and - in both ideal and realistic case - for two superlattices with one and five GaN/AlN pairs, respectively, in FIG. S4 of the supplementary material.

In conclusion, the cross-plane thermal conductivity of sapphire, GaN, and SLs consisting of up to 50 pairs of GaN/AlN has been investigated. The temperature dependent conductivity of various film thicknesses of GaN has been simulated and the values are reproduced by measuring the thermal conductivity with the differential 3ω -method. The simulated thermal conductivity of the GaN/AlN SL with different number of pairs has been compared and it is found that the change in absolute values is minimal. The measured values for SLs with individual layer thicknesses of 4 nm to 16 nm and 50 pairs increases at room temperature from 5.9 W/(m · K) to 10.1 W/(m · K). These results confirm the possibility of decreasing the cross-plane thermal conductivity of epitaxial crystalline GaN/AlN heterostructures to values as low as those reported for amorphous layers⁵⁵, opening wide perspectives for heat management in III-nitride-based devices.

See the supplementary material for the details about the epitaxial growth, the in depth TEM and XRD characterization and the simulations.

This work was supported by the European Commission's Horizon 2020 Research and Innovation Program [Grant No. 645776 (ALMA)] and by the Austrian Science Fund (FWF)

[Project P31423]. The authors thank Werner Ginzinger for preparing the specimens for the TEM experiments and for carrying out the related measurements, Heiko Groiss and Jesús Carrete for fruitful discussions, and Albin Schwarz for preparing the contact structures for the 3ω measurements.

DATA AVAILABILITY

The data that support the findings of this study are available from the corresponding author upon reasonable request.

This article may be downloaded for personal use only. Any other use requires prior permission of the author and AIP Publishing. This article appeared in A. Spindlberger *et al.*, Appl. Phys. Lett. 118, 062105 (2021) and may be found at <https://doi.org/10.1063/5.0040811>

- ¹F. Chen, X. Ji, and S. P. Lau, "Recent progress in group III-nitride nanostructures: From materials to applications," Mater. Sci. Eng. R Rep **142**, 100578 (2020).
- ²Y. Taniyasu and M. Kasu, "Polarization property of deep-ultraviolet light emission from C-plane AlN/GaN short-period superlattices," Appl. Phys. Lett. **99**, 251112 (2011).
- ³K. Kamiya, Y. Ebihara, K. Shiraishi, and M. Kasu, "Structural design of AlN/GaN superlattices for deep-ultraviolet light-emitting diodes with high emission efficiency," Appl. Phys. Lett. **99**, 151108 (2011).
- ⁴S. Nakamura, "Nobel Lecture: Background story of the invention of efficient blue InGaN light emitting diodes," Rev. Mod. Phys. **87**, 1139–1151 (2015).
- ⁵I. Akasaki, "Nobel Lecture: Fascinated journeys into blue light," Rev. Mod. Phys. **87**, 1119–1131 (2015).
- ⁶A. M. Dabiran, A. M. Wowchak, A. Osinsky, J. Xie, B. Hertog, B. Cui, D. C. Look, and P. P. Chow, "Very high channel conductivity in low-defect AlN/GaN high electron mobility transistor structures," Appl. Phys. Lett. **93**, 082111 (2008).
- ⁷L. Shen, S. Heikman, B. Moran, R. Coffie, N.-Q. Zhang, D. Buttari, I. Smorchkova, S. Keller, S. DenBaars, and U. Mishra, "AlGaIn/GaN high-power microwave HEMT," IEEE Electron Device Lett. **22**, 457–459 (2001).
- ⁸R. Adhikari, T. Li, G. Capuzzo, and A. Bonanni, "Controlling a three dimensional electron slab of graded $\text{Al}_x\text{Ga}_{1-x}\text{N}$," Appl. Phys. Lett. **108**, 022105 (2016).
- ⁹X. Li and X. Liu, "Group III nitride nanomaterials for biosensing," Nanoscale **9**, 7320–7341 (2017).
- ¹⁰T. Dietl, A. Bonanni, and H. Ohno, "Families of magnetic semiconductors — an overview," J. Semicond. **40**, 080301 (2019).
- ¹¹T. Dietl, K. Sato, T. Fukushima, A. Bonanni, M. Jamet, A. Barski, S. Kuroda, M. Tanaka, P. N. Hai, and H. Katayama-Yoshida, "Spinodal nanodecomposition in semiconductors doped with transition metals," Rev. Mod. Phys. **87**, 1311–1377 (2015).
- ¹²T. Devillers, L. Tian, R. Adhikari, G. Capuzzo, and A. Bonanni, "Mn as Surfaceant for the Self-Assembling of $\text{Al}_x\text{Ga}_{1-x}\text{N}/\text{GaN}$ Layered Heterostructures," Cryst. Growth Des. **15**, 587–592 (2015).
- ¹³R. Adhikari, M. Matzer, A. T. Martín-Luengo, M. C. Scharber, and A. Bonanni, "Rashba semiconductor as spin Hall material: Experimental demonstration of spin pumping in wurtzite $n\text{-GaN:Si}$," Phys. Rev. B **94**, 085205 (2016).
- ¹⁴X.-D. Wang, W.-D. Hu, X.-S. Chen, and W. Lu, "The Study of Self-Heating and Hot-Electron Effects for AlGaIn/GaN Double-Channel HEMTs," IEEE Trans. Electron Devices **59**, 1393–1401 (2012).
- ¹⁵S. A. Vitusevich, S. V. Danylyuk, N. Klein, M. V. Petrychuk, A. Y. Avksentyev, V. N. Sokolov, V. A. Kochelap, A. E. Belyaev, V. Tilak, J. Smart, A. Vertiatichikh, and L. F. Eastman, "Separation of hot-electron and self-heating effects in two-dimensional AlGaIn/GaN-based conducting channels," Appl. Phys. Lett. **82**, 748–750 (2003).
- ¹⁶D. G. Cahill, W. K. Ford, K. E. Goodson, G. D. Mahan, A. Majumdar, H. J. Maris, R. Merlin, and S. R. Phillpot, "Nanoscale thermal transport," J. Appl. Phys. **93**, 793–818 (2002).
- ¹⁷G. J. Snyder and E. S. Toberer, "Complex thermoelectric materials," Nat. Mater. **7**, 105–114 (2008).
- ¹⁸X. Fan, G. Zeng, C. LaBounty, J. E. Bowers, E. Croke, C. C. Ahn, S. Huxtable, A. Majumdar, and A. Shakouri, "SiGeC/Si superlattice microcoolers," Appl. Phys. Lett. **78**, 1580–1582 (2001).
- ¹⁹A. V. Inyushkin, A. N. Taldenkov, D. A. Chernodubov, V. V. Voronenkov, and Y. G. Shreter, "High Thermal Conductivity of Bulk GaN Single Crystal: An Accurate Experimental Determination," JETP Lett. (2020), 10.1134/S0021364020140039.
- ²⁰B. C. Daly, H. J. Maris, A. V. Nurmikko, M. Kuball, and J. Han, "Optical pump-and-probe measurement of the thermal conductivity of nitride thin films," J. Appl. Phys. **92**, 3820–3824 (2002).
- ²¹W. Liu and A. A. Balandin, "Temperature dependence of thermal conductivity of $\text{Al}_x\text{Ga}_{1-x}\text{N}$ thin films measured by the differential 3ω technique," Appl. Phys. Lett. **85**, 5230–5232 (2004).
- ²²B. Vermeersch, J. Carrete, and N. Mingo, "Cross-plane heat conduction in thin films with *ab-initio* phonon dispersions and scattering rates," Appl. Phys. Lett. **108**, 193104 (2016).
- ²³W. Liu and A. A. Balandin, "Thermal conduction in $\text{Al}_x\text{Ga}_{1-x}\text{N}$ alloys and thin films," J. Appl. Phys. **97**, 073710 (2005).
- ²⁴A. Filatova-Zalewska, Z. Litwicki, T. Suski, and A. Jeżowski, "Thermal conductivity of thin films of gallium nitride, doped with aluminium, measured with 3ω method," Solid State Sci. **101**, 106105 (2020).
- ²⁵J. Zou, X. Lange, and C. Richardson, "Lattice thermal conductivity of nanoscale AlN/GaN/AlN heterostructures: Effects of partial phonon spatial confinement," J. Appl. Phys. **100**, 104309 (2006).
- ²⁶P. P. Paskov, M. Slomski, J. H. Leach, J. F. Muth, and T. Paskova, "Effect of Si doping on the thermal conductivity of bulk GaN at elevated temperatures — theory and experiment," AIP Advances **7**, 095302 (2017).
- ²⁷R. L. Xu, M. Muñoz Rojo, S. M. Islam, A. Sood, B. Vareskic, A. Katre, N. Mingo, K. E. Goodson, H. G. Xing, D. Jena, and E. Pop, "Thermal conductivity of crystalline AlN and the influence of atomic-scale defects," J. Appl. Phys. **126**, 185105 (2019).
- ²⁸K. Park and C. Bayram, "Impact of dislocations on the thermal conductivity of gallium nitride studied by time-domain thermoreflectance," J. Appl. Phys. **126**, 185103 (2019).
- ²⁹A. Katre, J. Carrete, T. Wang, G. K. H. Madsen, and N. Mingo, "Phonon transport unveils the prevalent point defects in GaN," Phys. Rev. Mater. **2**, 050602 (2018).
- ³⁰Q. Zheng, C. Li, A. Rai, J. H. Leach, D. A. Broido, and D. G. Cahill, "Thermal conductivity of GaN, ^{71}GaN , and SiC from 150 K to 850 K," Phys. Rev. Mater. **3**, 014601 (2019).
- ³¹S. Zhang, X. Tang, H. Ruan, and L. Zhu, "Effects of surface/interface stress on phonon properties and thermal conductivity in AlN/GaN/AlN heterostructural nanofilms," Appl. Phys. A **125**, 732 (2019).
- ³²L. Zhu, X. Tang, J. Wang, and Y. Hou, "Modeling phonon thermal conductivity in spatially confined GaN nanofilms under stress fields and phonon surface scattering," AIP Advances **9**, 015024 (2019).
- ³³S.-S. Yang, Y. Hou, and L.-L. Zhu, "Effects of surface charges on phonon properties and thermal conductivity in GaN nanofilms," Chinese Phys. B **28**, 086501 (2019).
- ³⁴C. A. Polanco and L. Lindsay, "Phonon thermal conductance across GaN-AlN interfaces from first principles," Phys. Rev. B **99**, 075202 (2019).
- ³⁵D.-S. Tang, G.-Z. Qin, M. Hu, and B.-Y. Cao, "Thermal transport properties of GaN with biaxial strain and electron-phonon coupling," J. Appl. Phys. **127**, 035102 (2020).
- ³⁶A. van Rookeghem, B. Vermeersch, J. Carrete, and N. Mingo, "Thermal resistance of GaN/AlN graded interfaces," Phys. Rev. Applied **11**, 034036 (2019).
- ³⁷S. Mei and I. Knezevic, "Thermal conductivity of III-V semiconductor superlattices," J. Appl. Phys. **118**, 175101 (2015).
- ³⁸P. Chen, N. A. Katcho, J. P. Feser, W. Li, M. Glaser, O. G. Schmidt, D. G. Cahill, N. Mingo, and A. Rastelli, "Role of Surface-Segregation-Driven Interdiffusion on the Thermal Transport through Planar Si / Ge Superlattices," Phys. Rev. Lett. **111**, 115901 (2013).
- ³⁹L. Thumfart, J. Carrete, B. Vermeersch, N. Ye, T. Truglas, J. Feser, H. Groiss, N. Mingo, and A. Rastelli, "Thermal trans-

- port through Ge-rich Ge/Si superlattices grown on Ge(0 0 1)," J. Phys. D: Appl. Phys. **51**, 014001 (2018).
- ⁴⁰Y. Feng and X. Liang, "Modified series model for cross-plane thermal conductivity of short-period Si/Ge superlattices," Sci. China Phys. Mech. Astron. **58**, 1–8 (2015).
- ⁴¹Y. K. Koh, Y. Cao, D. G. Cahill, and D. Jena, "Heat-Transport Mechanisms in Superlattices," Adv. Funct. Mater. **19**, 610–615 (2009).
- ⁴²D. G. Cahill, "Thermal conductivity measurement from 30 to 750 K: The 3 ω method," Rev. Sci. Instrum. **61**, 802–808 (1990).
- ⁴³S.-M. Lee and D. G. Cahill, "Heat transport in thin dielectric films," J. Appl. Phys. **81**, 2590–2595 (1997).
- ⁴⁴A. Kaminska, P. Strak, J. Borysiuk, K. Sobczak, J. Z. Domagala, M. Beeler, E. Grzanka, K. Sakowski, S. Krukowski, and E. Monroy, "Correlation of optical and structural properties of GaN/AlN multi-quantum wells—Ab initio and experimental study," J. Appl. Phys. **119**, 015703 (2016).
- ⁴⁵C. Zhang, R. ElAfandy, and J. Han, "Distributed Bragg Reflectors for GaN-Based Vertical-Cavity Surface-Emitting Lasers," Appl. Sci. **9**, 1593 (2019).
- ⁴⁶M. Shan, Y. Zhang, T. B. Tran, J. Jiang, H. Long, Z. Zheng, A. Wang, W. Guo, J. Ye, C. Chen, J. Dai, and X. Li, "Deep UV Laser at 249 nm Based on GaN Quantum Wells," ACS Photonics **6**, 2387–2391 (2019).
- ⁴⁷C. Gusenbauer, T. Ashraf, J. Stangl, G. Hesser, T. Plach, A. Meingast, G. Kothleitner, and R. Koch, "Interdiffusion in Heusler film epitaxy on GaAs(001)," Phys. Rev. B **83**, 035319 (2011).
- ⁴⁸J. Garg and G. Chen, "Minimum thermal conductivity in superlattices: A first-principles formalism," Phys. Rev. B **87**, 140302 (2013).
- ⁴⁹S. C. Huberman, J. M. Larkin, A. J. H. McGaughey, and C. H. Amon, "Disruption of superlattice phonons by interfacial mixing," Phys. Rev. B **88**, 155311 (2013).
- ⁵⁰H. Li, T. Wang, Y. Liu, J. Ao, and S. Sakai, "V-Shaped Defects in Al-GaN/GaN Superlattices Grown on Thin Undoped-GaN Layers on Sapphire Substrate," Jpn. J. Appl. Phys. **41**, L732 (2002).
- ⁵¹T. Tong and A. Majumdar, "Reexamining the 3-omega technique for thin film thermal characterization," Rev. Sci. Instrum. **77**, 104902 (2006).
- ⁵²S. Burghartz and B. Schulz, "Thermophysical properties of sapphire, AlN and MgAl₂O₄ down to 70 K," J. Nucl. Mater. **212-215**, 1065–1068 (1994).
- ⁵³D. G. Archer, "Thermodynamic Properties of Synthetic Sapphire (Al₂O₃), Standard Reference Material 720 and the Effect of Temperature-Scale Differences on Thermodynamic Properties," J. Phys. Chem. Ref. Daten **22**, 1441–1453 (1993).
- ⁵⁴J. Carrete, B. Vermeersch, A. Katre, A. van Roekeghem, T. Wang, G. K. Madsen, and N. Mingo, "almaBTE: A solver of the space-time dependent Boltzmann transport equation for phonons in structured materials," Comput. Phys. Commun. **220**, 351–362 (2017).
- ⁵⁵H. Mizuno, S. Mossa, and J.-L. Barrat, "Beating the amorphous limit in thermal conductivity by superlattices design," Sci. Rep. **5**, 14116 (2015).
- ⁵⁶G. Chen, "Thermal conductivity and ballistic-phonon transport in the cross-plane direction of superlattices," Phys. Rev. B **57**, 14958–14973 (1998).
- ⁵⁷J. Carrete, B. Vermeersch, L. Thumfart, R. R. Kakodkar, G. Trevisi, P. Frigeri, L. Seravalli, J. P. Feser, A. Rastelli, and N. Mingo, "Predictive Design and Experimental Realization of InAs/GaAs Superlattices with Tailored Thermal Conductivity," J. Phys. Chem. C **122**, 4054–4062 (2018).

Cross-plane thermal conductivity of GaN/AlN superlattices: Supplementary Material

Anna Spindlberger,^{a)} Dmytro Kyslychyn, Lukas Thumfart, Rajdeep Adhikari, Armando Rastelli, and Alberta Bonanni^{a)}

Institute of Semiconductor and Solid-State Physics, Johannes Kepler University Linz, Altenbergerstr. 69, 4040 Linz, Austria

(Dated: 14 October 2021)

I. EPITAXIAL GROWTH

The investigated samples are fabricated in an AIXTRON 200RF horizontal tube metal organic vapor phase epitaxy (MOVPE) reactor on *c*-plane sapphire substrates. As precursors TMGa, TMAI and NH₃ for Ga, Al and N respectively are used and H₂ as carrier gas. The flow rates are kept constant at 25 standard cubic centimeters per minute (sccm) for Ga and Al and 1500 sccm for NH₃ at the whole growth process. First the substrate is heated to 1080 °C and floated with ammonia for nitridation, then a thin GaN nucleation layer is grown at 540 °C and annealed at 1040 °C. The growth continues with a 1.5 μm thick buffer layer of GaN and for the GaN/AlN heterostructure 50 pairs of GaN on AlN layers are deposited. For this study, the thicknesses of the individual superlattice (SL) layers varies from 4 nm to 16 nm over the samples' series. The growth process is monitored *via in-situ* reflectometry.

II. DETAILS ON CHARACTERIZATION

A. X-ray diffraction

High-resolution x-ray diffraction (HRXRD) has been carried out with a PANalytical's X'Pert PRO Materials Research Diffractometer (MRD) equipped with a hybrid monochromator with a 1/4° divergence slit. The MRD includes a PixCel detector with 256-channels and a 11.2 mm anti-scatter slit. To gain insights in the relaxation of the samples, reciprocal space maps (RSM) are performed at the (105) diffraction peak of GaN. The most prominent peak in the RSM in FIG. S1 (a) for SL4 is due to the GaN buffer. The fringes around this peak, are due to the 50 pairs of GaN/AlN and the SL in all considered samples exhibit ~ 50% relaxation on to the GaN buffer layer (different Q_x value for the peaks of the fringes). Moreover, $\omega - 2\theta$ scans are performed, where the thickness fringes of the SL can be seen. The fringes are reproduced by simulating the $\omega - 2\theta$ signal of the SL with the AMASS software from PANalytical and fitting the measured signal. Due to interdiffusion between the AlN and GaN layer, a graded Al_xGa_{1-x}N layer of thickness d_{AlGa} between the two SL layers is considered in the simulation. The fitted thicknesses and Al concentrations of each layer are summarized in Table S1

TABLE S1. Fitted layer thicknesses of the SL layers and the inter-diffusion region (d_{AlGa}).

sample	d_{GaN} (nm)	d_{AlN} (nm)	d_{AlGa} (nm)
SL4	4.09	2.22	1.18
SL8	10.00	0.82	5.01
SL12	13.88	3.99	8.68

and an example simulation is given in FIG. 1 (a) of the main text. The measurement exhibit broader peaks than the simulation.

B. Transmission Electron Microscopy

The transmission electron microscope (TEM) used in this study is a JEOL JEM-2200FS TEM microscope operated at 200 kV in conventional and high-resolution imaging (HRTEM) modes. The preparation of the TEM specimens, both cross-section and plan-view, is done by a conventional procedure of mechanical polishing followed by Ar⁺ milling and double-side plasma cleaning. For the elemental analysis, energy dispersive x-ray spectroscopy (EDX) is performed while measuring the samples in scanning TEM mode (STEM). To gain a broad overview of the sample structure high-angle annular dark-field imaging (HAADF) is also conducted.

In the HAADF images, the individual layers of the SL are visible, as in FIG. S2 (a) for SL12. The sample contains defects extending from the GaN buffer to the surface. By comparing SL12 to the SL4 given in FIG. 1 (b) of the main text, an increase in defect density is found for the SL12. These defects are most prominent in the SL16 (not shown). FIG. S2 (c) gives a detailed view of one those V-shaped defects¹. In the V-pits GaN is preferably accumulated. In the investigated structures inverted V-pits (anti-parallel to the growth direction) are found, as for example in FIG. S2 (d). In FIG. S2 (b), a HAADF plane view of SL16 is provided. The EDX measurements shown in FIG. S3 (a) for SL4 and (b) for SL8 confirm the alternate presence of Ga and Al in the SL layers. Between the AlN and GaN an interdiffusion region is detected.

^{a)} Authors to whom correspondence should be addressed: anna.spindlberger@jku.at and alberta.bonanni@jku.at

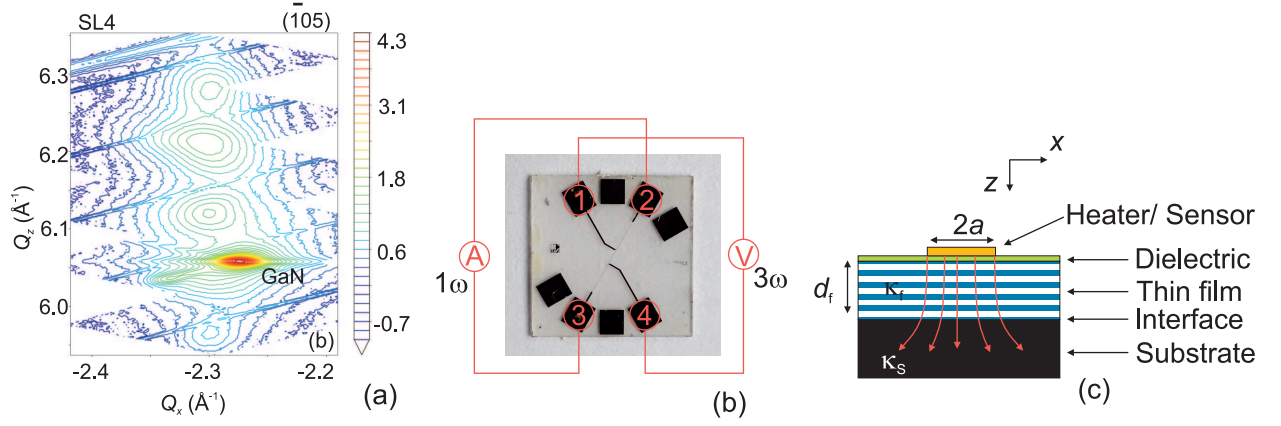


FIG. S1. (a) RSM around the $(\bar{1}05)$ peak of GaN of SL4. (b) Geometry used for the differential 3ω measurements with contact pads for current I and voltage V (c) Schematic sample structure of the SL with overall thermal film conductivity κ_f and substrate conductivity κ_s

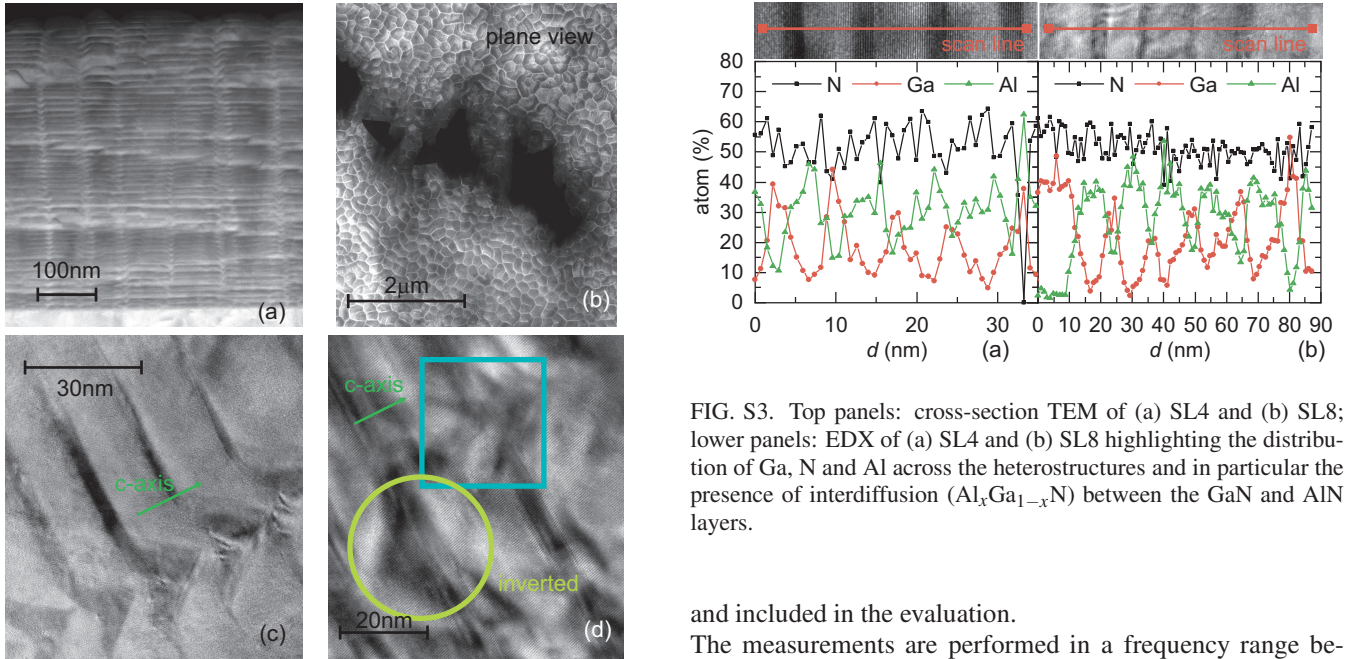


FIG. S2. (a) HAADF image of SL12. (b) Plane view of SL16 (c) Magnification of a region with V shape defects of SL12 and (d) with inverted V shape.

C. Thermal conductivity with the 3ω -method

The cross-plane thermal conductivity κ_{\perp} is measured with the differential 3ω -method^{2,3} for temperatures between 160 K to 455 K. For this method, a 60 nm thick AlO_x is deposited by atomic layer deposition, followed by several lithography steps to define the heater geometry shown in FIG. S1 (b). The heater geometry consists of a 5 nm thin Cr adhesion layer followed by a 120 nm thick Au layer, fabricated by metal deposition. The strip width is chosen to be $2a = 10\mu\text{m}$ and this strip acts as both heater and thermometer. The heater thickness is confirmed by atomic force microscopy

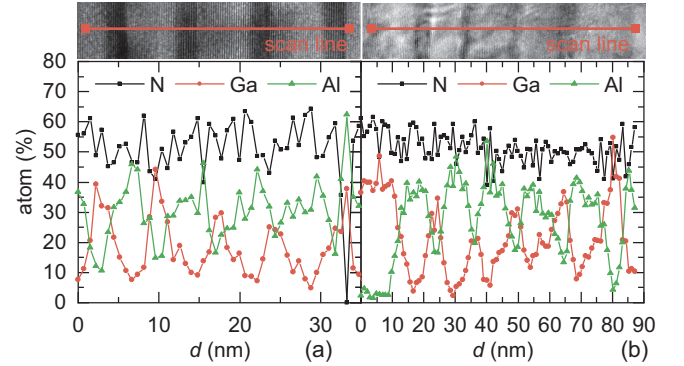


FIG. S3. Top panels: cross-section TEM of (a) SL4 and (b) SL8; lower panels: EDX of (a) SL4 and (b) SL8 highlighting the distribution of Ga, N and Al across the heterostructures and in particular the presence of interdiffusion ($\text{Al}_x\text{Ga}_{1-x}\text{N}$) between the GaN and AlN layers.

and included in the evaluation.

The measurements are performed in a frequency range between 40 Hz and 4000 Hz and a power per unit length of 15 W/m .

The values of the thermal conductivity are obtained by fitting the measured data and by solving the diffusion equation, *i.e.* by calculating the two dimensional heat flow of a multilayer structure with the transfer matrix method. The fitting routine first treats the sapphire substrate and the buffer layer and then the SL is included as an additional thin film.

III. THEORETICAL APPROACH

A. AlmaBTE software

With the almaBTE software package the phonon transport for bulk crystals or alloys, thin films and also multilayered structures can be calculated. The software solves the space- and time-dependent Boltzmann transport equation (BTE)

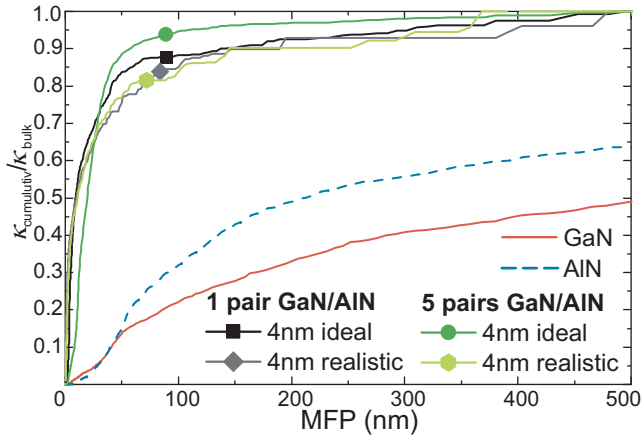


FIG. S4. Simulated cumulative thermal conductivity normalized to the bulk over the phonon mean free path for bulk GaN, bulk AlN, and for one pair and five pairs of GaN/AlN in the ideal and realistic case.

and calculates the thermal conductance, the effective thermal conductivities and heat-current distributions⁴.

In contrast to Monte Carlo methods, the *almaBTE* solver starts with a pre-calculated equilibrium component of the material and after building the desired structure calculates the phonon transport and the related quantities. Several materials are already included in the materials catalog and can be downloaded from the homepage www.almaBTE.eu. The material files include information about the geometrical description and the second- and third-order derivatives of its potential energy at equilibrium⁴.

The package includes the temperature independent 2-phonon scattering rates, elastic scattering rates and at each temperature the resulting 3-phonon scattering rates. With the

relaxation time approximation each component of the thermal conductivity tensor is obtained in dependence on the mode contribution of the heat capacity, the volumetric heat capacity, the mean free path and the group velocity.

Concerning the simulations, for a SL with 4 nm individual layer thickness and one pair, the ideal SL contains eight monolayers of GaN and eight monolayers of AlN. Whereas for a realistic SL six monolayers of GaN and AlN are included and intercalated four monolayers of $\text{Al}_x\text{Ga}_{1-x}\text{N}$ with x ranging from zero to one are included. For higher number of pairs, the procedure is repeated. In the case of realistic SLs the interdiffusion between each GaN and AlN layer is included.

In FIG. S4 the simulated cumulative thermal conductivity normalized to the bulk is provided as a function of the mean free path (MFP) of the phonons for bulk AlN, bulk GaN, and – in both ideal and realistic case – for two superlattices with one and five GaN/AlN pairs, respectively. For the heterostructures (ideal and realistic), the main contribution to the thermal conductivity is given by phonons with MFP lower than 400 nm. In contrast, in the bulk GaN and AlN only half of the total thermal conductivity is transported by phonons with MFP lower than 500 nm. It is worth mentioning, that Carrete *et al.*⁴ reported a MFP up to 10 μm for the two bulk materials.

¹H. Li, T. Wang, Y. Liu, J. Ao, and S. Sakai, “V-Shaped Defects in Al-GaN/GaN Superlattices Grown on Thin Undoped-GaN Layers on Sapphire Substrate,” *Jpn. J. Appl. Phys.* **41**, L732 (2002).

²D. G. Cahill, “Thermal conductivity measurement from 30 to 750 K: The 3ω method,” *Rev. Sci. Instrum.* **61**, 802–808 (1990).

³S.-M. Lee and D. G. Cahill, “Heat transport in thin dielectric films,” *J. Appl. Phys.* **81**, 2590–2595 (1997).

⁴J. Carrete, B. Vermeersch, A. Katre, A. van Roekeghem, T. Wang, G. K. Madsen, and N. Mingo, “*almaBTE*: A solver of the space-time dependent Boltzmann transport equation for phonons in structured materials,” *Comput. Phys. Commun.* **220**, 351–362 (2017).